

Numerical Comparison of the Parameters Influencing the Turbulent Flow using a T-shaped Spur Dike in a 90° Bend

M. Vaghefi[†], Y. Safarpour and M. Akbari

Civil Engineering Department, Persian Gulf University, Bushehr, 7516913817, Iran

[†]Corresponding Author Email: vaghefi@pgu.ac.ir

(Received February 3, 2016; accepted August 9, 2016)

ABSTRACT

Spur dikes are used for river training purposes. To meet the navigability of rivers, the mean annual flow is considered; hence, in terms of river flooding, spur dikes are necessarily submerged. Considering the importance of submerged spur dikes, this paper studied the effects of a T-shaped spur dike's submergence ratios on turbulent flow parameters in a 90° bend using the SSIIM as a commercial CFD model. The SSIIM numerical model solves the Navier-Stokes equations with the $k-\epsilon$ model on a three-dimensional, almost general, non-orthogonal grid. Submergence ratios of 0 (non-submerged), 5, 15, 25 and 50% were evaluated for parameters affecting the turbulent flow such as kinetic energy, pressure, eddy viscosity and the Froude number. It was observed that by increasing the spur dike submergence ratio from 0% (non-submerged) to 50%, in addition to changes in the values of pressure and kinetic energy, the Froude number changed in the bend and increased 2.1 times at the inner bank of the bend exit, and the eddy viscosity near the bed, which is the decisive factor of the turbulent flow, reduced by 42%. At the bed near the spur dike wing, the amount and range of kinetic energy reduced by increasing the submergence ratio. Near the bed, for all submergence ratios, the maximum pressure occurred at the upstream end of the spur dike.

Keywords: Froude number; Kinetic energy; SSIIM model; Turbulent flow.

NOMENCLATURE

k	kinetic energy	U^*	shear velocity
ks	roughness	ν_T	eddy viscosity
l	length of spur dike wing		
L	length of spur dike web	δ_{ij}	Kronecker delta
P	pressure	ϵ	loss of kinetic energy
U	velocity		

1. INTRODUCTION

A spur dike serves to train the stream flow, protect the stream bank from erosion and improve the depth for navigation. Spur dikes have been studied intensively for many years mostly as river-training or river-rehabilitation structures (Vaghefi *et al.*, 2015). Spur dikes may be either submerged or non-submerged, depending on the objectives and conditions of the river. In sand-bed and meandering rivers, the impermeable spur dike with crest height at the level of upper wall of the main river are used to protect the banks. These spur dikes are submerged necessarily at times of greater floods and by extending flow in the river floodplain.

The study of flow pattern and sediment transport in rivers and protecting their walls against high velocity in straight and bend routs is of high importance; therefore, researchers have conducted a large number of studies regarding this subject with and without placing a spur dike on the route. Shukry (1950) studied the flow around the bends in an open flume and presented an equation for determination of the secondary flow strength. Rajaratnam and Nwachukwu (1983) studied the structure of turbulent flow near groin-like structures. Mayerle *et al.* (1995) reviewed the effect of hydrostatic pressure to model flow pattern around the spur dike. They also reviewed the effect of the wall boundary conditions on the flow velocity using a numerical model and obtained a hydrostatic pressure distribution that

explains the difference in the flow pattern near the spur dike. Sukhodolov *et al.* (2004) studied turbulent flow and sediment distributions in a groyne field. McCoy (2006) presented a detailed numerical study using fully three-dimensional Large Eddy Simulation (LES) of the flow and mass exchange processes in straight channels containing one or multiple embayments with vertical spanwise walls on one side corresponding to the presence of groynes in river reaches. Fazli *et al.* (2008) did an experimental study on a 90 degree bend channel to study the parameters affecting scour around short and straight spur dikes. The results indicate that in developed bends, as the spur dike is moved away from the beginning of the bend, maximum scour depth rises. Zhang *et al.* (2009) investigated the turbulent flow in the local scour hole around a single non-submerged spur dike via both experimental and numerical methods. Yazdi *et al.* (2010) discovered that the maximum bed shear stress can be seen in vertical spur dikes rather than for spur dikes oriented upstream or downstream. Abhari *et al.* (2010) used the $k-\epsilon$ model to predict the turbulence of flow in a 90 degree bend; comparison between the experimental data and numerical model showed that the SSIIM model is able to simulate the flow pattern accurately. Vaghefi *et al.* (2009-2012) conducted some experimental studies on the effect of T-shaped spur dike length on scour in a 90 degree channel bend and discovered that with increase in the length of spur dike, the height of the ridge increases at the downstream end of the spur dike. They conducted an experimental study on scour around a T-shaped spur dike in a channel bend, and showed that the dimension of the scour hole increases by increasing the length of the spur dike, decreasing the wing length of spur dike, increasing the Froude number and changing the location of spur dike towards downstream. They also studied the effect of Froude number on the flow pattern and scouring around a T-shaped spur dike in a 90 degree bend and concluded that by increasing the Froude number, the stress concentration will be more in constriction section. The distance of the second scour hole from the spur dike increases by increasing the Froude number. Duan *et al.* (2011) measured three-dimensional flow field around a dike structure using a micro ADV. They studied turbulent bursts around the spur dike for the flat and asymptotic bed surface. Fang *et al.* (2013) studied the turbulent flow past a series of groins in a shallow, open channel by LES. Their model results showed that a rectangular-headed groin generates higher turbulence intensities and larger vortices than a round-headed groin. Vaghefi *et al.* (2014) studied the effect of the Froude number on the flow field around a submerged T-shaped spur dike using the FLOW-3D software and concluded that as the Froude number increases, the flow behind the wing of the spur dike changes from down flow into up flow. With an increase in Froude number, the vortices become 35% smaller. Vaghefi *et al.* (2015) studied the effects of relative curvature of bend on scour pattern due to installation of a T-

shaped spur in a 90 degree channel bend with mobile bed. Basser *et al.* (2015) proposed a new approach to determine optimum parameters of a protective spur dike to mitigate scouring depth amount around existing main spur dikes. Vaghefi *et al.* (2016) conducted an experimental study on Reynolds shear stress and turbulent kinetic energy in a 180 degree sharp bend. They concluded that the maximum of these parameters occur in the first half the bend and near inner wall.

As seen, most of the researches have been conducted on the mean flow and scour patterns in rivers. In this study, given the importance of turbulent flow parameters' effect on the variations in flow and scour patterns, these parameters were compared based on the submergence ratio of T-shaped spur dike using the numerical model in a 90 degree bend.

2. MATERIALS AND METHODS

2.1 Experimental Model

The experiments have been carried out in the Hydraulics Laboratory of Tarbiat Modares University in Iran (Vaghefi *et al.*, 2012). According to Fig. 1, the laboratory flume includes a compound of direct and bend routes with width of 60 cm, and the height of 70 cm. The straight upstream route is 710 cm long, and is connected to a 520-centimeter-long, straight downstream route via a 90 degree bend with an external radius of 270 cm, and an internal radius of 210 cm. The ratio of bend radius to channel width is 4 (R_c/B). Uniform sediments have an average diameter of 1.28 mm and the standard deviation is 1.3; also the flow discharge throughout the experiment is held constant, equal to 25 L/s, and the sediment particles specific gravity (G) is equal to 2.35. The flow depth is equal to 11.6 cm at the entrance of the bend. Accordingly, the Froude number is also equal to 0.34 in the upstream straight route. Also, drinking water is used in the experimental modeling. The flow measurement was done by the Vectrino velocimeter at different cross sections and for several horizontal layers. The velocity at each point was measured by sampling rate of 50 Hz for a period of one to three minutes and time averaged velocities were calculated.

The spur dike used in these experiments is a T-shaped spur dike. The spur dike is made of Plexiglas wings of 90 degree rounded corners. The length of wing (l) and that of web (L) are the same and equal to 9 cm, with the height of 25 cm. This spur dike is vertical and non-submerged in a 45 degree position, and is located in the external bend. Clear water conditions govern the flow in experiments. Since, the maximum scour occurs in clear water conditions because sediment does not flow at the channel's upstream and the upstream sediment discharge does not result in filling the scour holes. Also, the channel walls are rigid and the erosion takes place only through the channel bed. Because if the wall is not rigid, the erosion created at the walls lead to variations in water height on the spur dike crest.

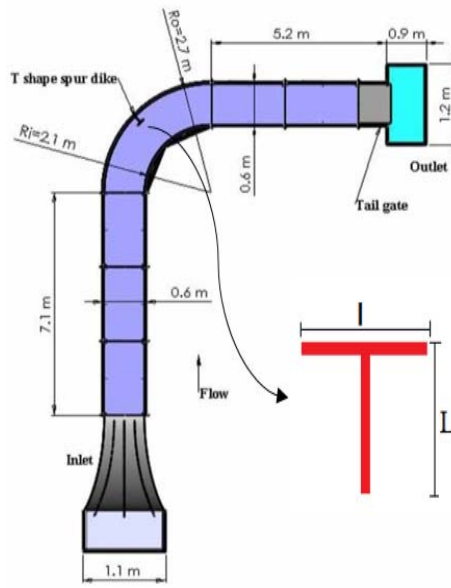


Fig. 1. Laboratory flume and spur dike.

2.2 Numerical Model

SSIIM is the abbreviation for Sediment Simulation In Intakes with a Multi block option. The SSIIM numerical model solves the Navier-Stokes equations (Elçi and Ekmekçi, 2016) with the $k-\epsilon$ model (Falahatkar and Ahmadikia, 2014) on a three-dimensional, almost general, non-orthogonal grid. The SIMPLE (Semi-Implicit Method for Pressure Linked Equations) method is the default method used for pressure-correction. To calculate the Reynolds stress term, the program makes use of the turbulence model. Therefore the kinetic energy of the turbulent flow is characterized based on the flow velocity. The cinematic viscosity is the fluid properties while the eddy viscosity depends on the velocity and is expressed to introduce the Reynolds stress. This program does not consider density variations due to salinity variations. The SIMPLE method can be used for the equations of interlinked pressures. The main purpose of this method is to estimate and determine a value for the pressure and replace it by the continuity equation and obtain the pressure correction factor (Olsen, 2000-2001). The ability to run the SSIIM model on personal computers was the reason why it was accepted as a design tool for water and environmental related engineering (Wildhagen, 2004).

The Navier-Stokes equations for turbulent flow in a general three-dimensional geometry are solved to obtain the water velocity. The Navier-Stokes equations for non-compressible and constant density flow can be modeled as Eq. (1), where x_1 , x_2 and x_3 are distances and U_1 , U_2 and U_3 are velocities in three directions. P is pressure and δ_{ij} is Kronecker delta that is equal to unity for $i = j$ and is zero otherwise. The left term on the left side of the equation is the transient term. The next term is the convective term. The first term on the right-hand side is the pressure term. The second term on the right side of the equation is the Reynolds stress term (Olsen, 2009).

$$\frac{\partial U_i}{\partial t} + U_j \frac{\partial U_i}{\partial x_j} = \frac{1}{\rho} \frac{\partial}{\partial x_i} (-P\delta_{ij} - \overline{\rho u_i u_j}) \quad (1)$$

The grid systems in the vertical, lateral and longitudinal directions have 26, 70 and 36 lines respectively. The mesh size near the spur dike is smaller so that better results may be obtained. Fig. 2 shows a schematic view of the grids used in plan and around spur dike in the numerical model.

The analysis for submergence ratios of 0, 5, 15, 25, and 50% has been conducted and the results were integrated. Duration of analysis of each submergence ratio is about 8 hours for the flow and scour patterns. As a boundary condition, the discharge was introduced in the bend entrance. The gradient of all parameters in the outputs boundary is zero. In addition, the output rates of discharge must be introduced in the outgoing boundary conditions. Gradient of kinetic energy loss as well as the value of kinetic energy at the water surface is zero. The flux passing the bed and walls is zero. The velocity profile follows a certain empirical function, called a wall law as Eq. (2), where U is velocity, U^* shear velocity, k a constant coefficient equal to 0.4, y the distance from the wall to the center of the cell, and k_s the roughness, that is equal to 90% of particles diameter in the bed grading curve (Olsen, 1999).

$$\frac{U}{U^*} = \frac{1}{k} \ln \left(\frac{30 y}{k_s} \right) \quad (2)$$

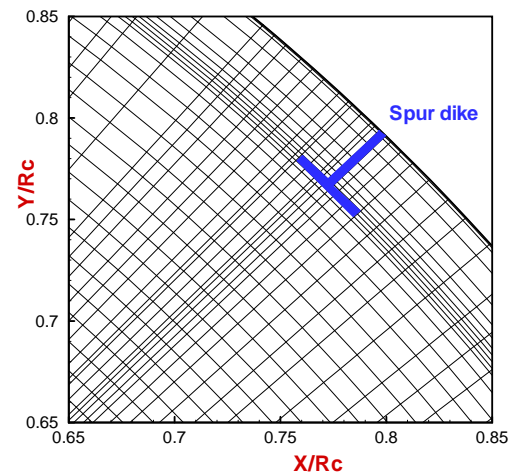


Fig. 2. A schematic view of grid used in the channel with T-shaped spur dike.

3. RESULT AND DISCUSSIONS

To reach better results and verify the numerical model, the numerical model was calibrated using Vaghefi *et al.* (2012) experimental model results (Froude number equals to 0.34). The comparisons of longitudinal velocities for both models at different cross sections of 40 and 60 degrees (these locations are at the upstream and downstream ends of the spur dike, respectively) are shown in Fig. 3. According to this figure, it is observed that the experimental and numerical

data are almost the same and this indicates that the SSIIM model is capable of providing the bed's changes and three-dimensional velocities and is well approximated by the laboratory model. In other words, the numerical model could accurately simulate the flow and scour patterns in a bend containing a hydraulic structure such as spur dike.

$$k = 1/2(u'^2 + v'^2 + w'^2) \quad (3)$$

$$\frac{\partial k}{\partial t} + U_j \frac{\partial k}{\partial x_j} = \frac{\partial}{\partial x_j} \left(\frac{v_T}{\sigma_k} \frac{\partial k}{\partial x_j} \right) + P_k - \varepsilon \quad (4)$$

$$P_k = v_T \frac{\partial U_j}{\partial x_i} \left(\frac{\partial U_j}{\partial x_i} + \frac{\partial U_i}{\partial x_j} \right) \quad (5)$$

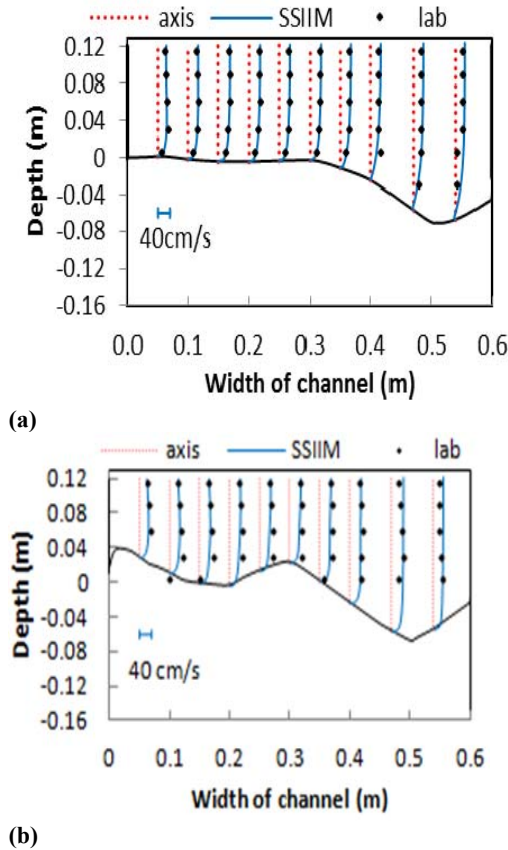


Fig. 3. Longitudinal velocities in experimental and numerical models at: (a) $\theta = 40^\circ$, and (b) $\theta = 60^\circ$.

The comparison between numerical and experimental velocity data in horizontal direction at the plan near water surface is presented in Fig. 4. In this figure, the accordance between the two numerical and experimental models is more evident after the location of the spur dike near the outer wall, because, highly turbulent flow condition is present at the spur dike area.

3.1 Kinetic Energy

To calculate the Reynolds stress term, the program uses the $k-\varepsilon$ model. Therefore, the kinetic energy of the turbulent flow model is characterized based on the flow velocity. The balance of the turbulent kinetic energy is defined as Eqs. (3) and (4), where u' , v' , and w' are velocities in three dimensions (Wildhagen, 2004; Olsen, 2009). $k-\varepsilon$ and v_T are respectively the kinetic energy, the loss of kinetic energy, and the eddy viscosity. P_k is defined as Eq. (5).

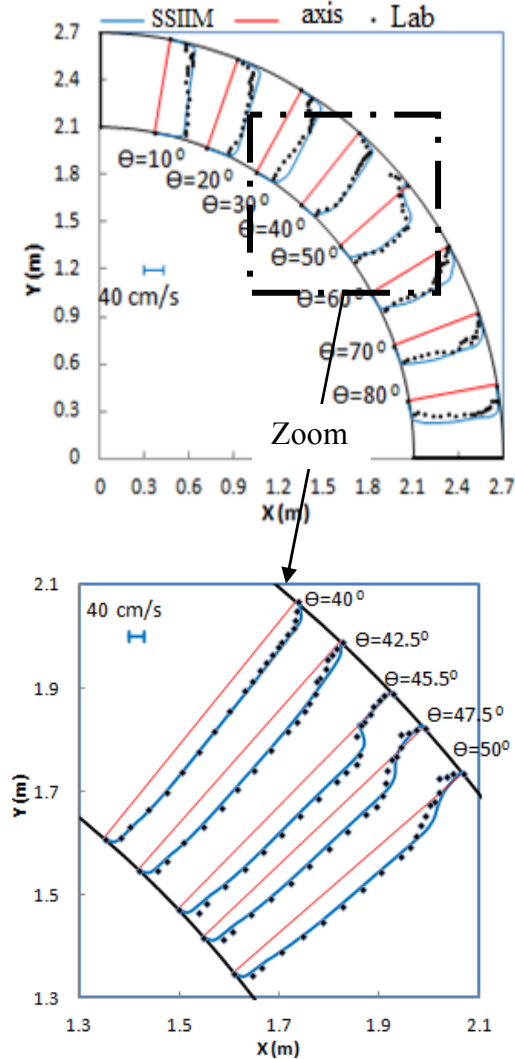


Fig. 4. Comparing of horizontal velocities near the water surface in experimental and numerical models.

At the upstream end of the spur dike, the flow is divided into two categories, one moving towards the surface, and the other towards the bed. The stream lines are deflected downward after hitting the spur dike. After hitting the bed, the down flow has dug a hole on the nose of the spur dike. A rotating flow is then created inside the hole, which in turn causes a gradual increase in the hole depth, continuing to achieve balance. As shown in Figs. 5 and 6, the kinetic energy changes are affected by submergence ratio. At the bed near the wing of the spur dike, by increasing the submergence ratio, the amount and range of changes of kinetic energy decrease.

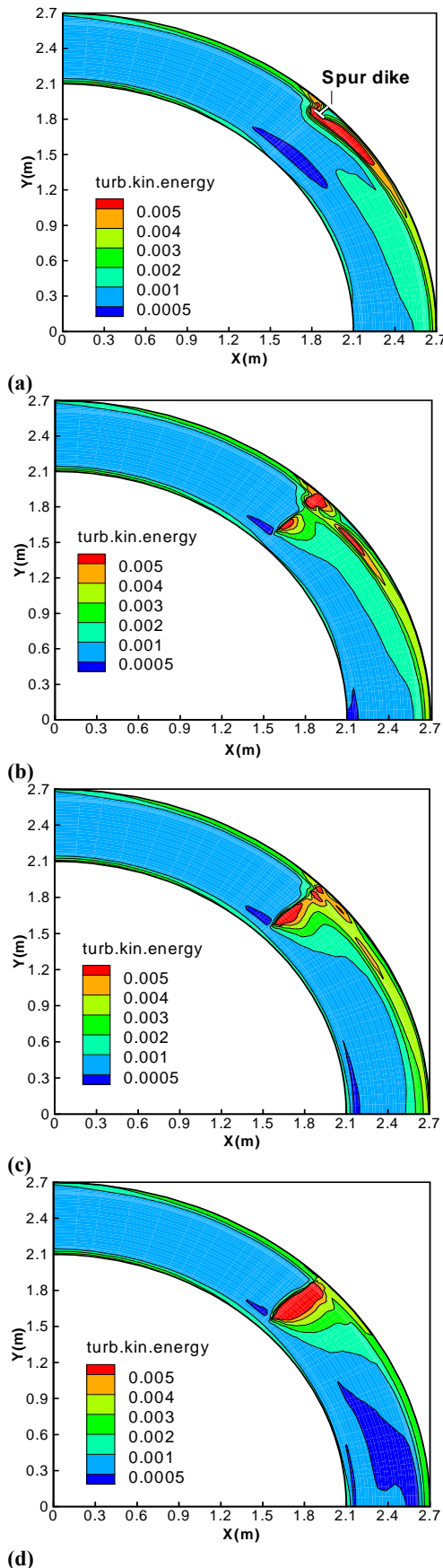


Fig. 5. Kinetic energy on water surface at submergence ratios of: (a) 0%, (b) 5%, (c) 25%, and (d) 50%.

The kinetic energy zone increases at the water surface by spur dike submergence, due to changes in the flow velocity through the spur dike crest level which continues to the inner bank. Yet the maximum amount of the kinetic energy zone on the water surface becomes larger and extends toward the inner bank and the location of the spur dike, because by increasing the spur dike submergence, more current passes through the crest level of spur dike and the kinetic energy increases in that zone. Also, by increasing the submergence ratio, the maximum kinetic energy zone decreases near the spur dike axis at the bed; because the effects of downward flows are slower near the bed. By simulating flow and scour field around the T-shaped spur dikes at different submergence ratios, Vaghefi *et al.* (2015) concluded that while the submergence ratio grows from 5% to 50%, the maximum amount of scour is reduced. This is due to decrease in the effect of the T-shaped spur dike wing on transverse flow diversion.

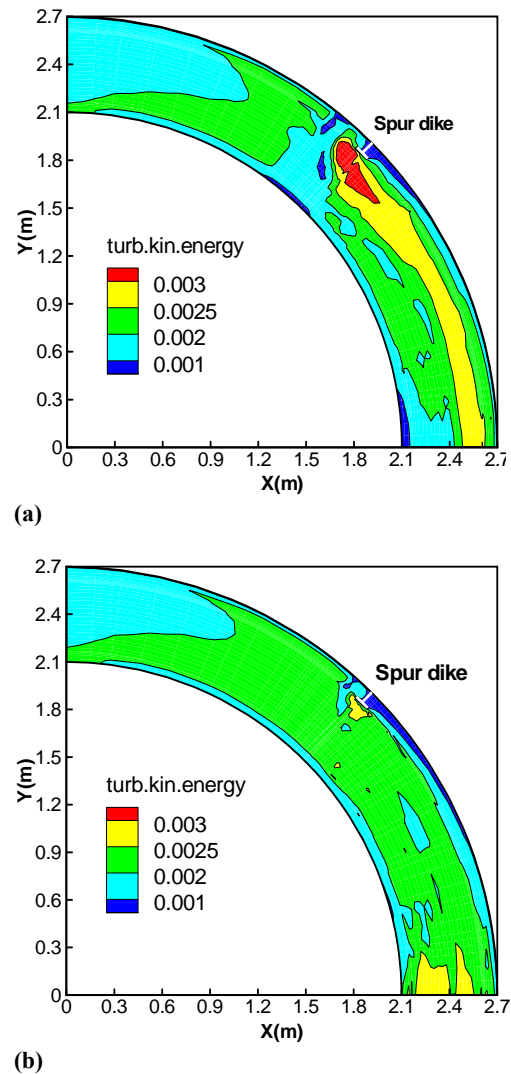


Fig. 6. Kinetic energy near the bed at submergence ratios of: (a) 0%, and (b) 50%.

3.2 Loss of Kinetic Energy

The loss of kinetic energy is denoted by ϵ , which is applicable to state the eddy viscosity and defined as Eq. (6). In the above equations, in $k-\epsilon$ model, the constants are equal to the following values (Olsen, 2009):

$$\frac{\partial \epsilon}{\partial t} + U_j \frac{\partial \epsilon}{\partial x_j} = \frac{\partial}{\partial x_j} \left(\nu_T \frac{\partial \epsilon}{\partial x_j} \right) + C_{\delta 1} \frac{\epsilon}{\kappa} P_\kappa + C_{\delta 2} \frac{\epsilon^2}{\kappa} \quad (6)$$

$$\sigma_\epsilon = 1.3 \quad C_{\delta 1} = 1.44 \quad C_{\delta 2} = 1.92$$

As shown in Figs. 7 and 8, the changes in the loss of kinetic energy are shown as affected by submergence ratios on the water surface and closely near the bed. It is observed that variation in the loss of kinetic energy is minimal before the spur dike location. Near the bed, by increasing the submergence ratio, the maximum loss of changes in kinetic energy is minimized in the middle of channel, at a distance ranging from the downstream end of the spur dike to the bend exit, and the changes are limited to the location of the spur dike. In other words, the zone of kinetic energy loss rises at the inner bank. On the water surface, upon spur dike submergence, the loss of kinetic energy increases at the outer bank, and by increasing the submergence ratio, the loss of kinetic energy increases on the water surface and between the spur dike location to the inner bank due to changes on the flow velocity affected by the subcritical flow passing over the spur dike crest level and the sudden change of flow depth.

3.3 Eddy Viscosity

The cinematic viscosity is of fluid properties while the eddy viscosity depends on the velocity and is expressed to introduce the Reynolds stress. The model calculates the eddy viscosity as Eq. (7), where k is the kinetic energy of the turbulent flow, ϵ is the loss of kinetic energy of the turbulent flow, and $C_\mu = 0.09$ (Olsen, 2009).

$$\nu_T = C_\mu \frac{k}{\epsilon} \quad (7)$$

As in Figs. 9-12 and in all submergence ratios near the bed, the maximum eddy viscosity occurs near the upstream wing of the spur dike and its minimum is at the end of the outer bank. Eddy viscosity is higher at the water surface than on the bed because of increase in the water velocity at higher levels.

At water surface, in all submergence ratios, the maximum eddy viscosity occurs at the upstream wing of the spur dike and at the second half of the bend near the outer bank. Its minimum occurs near the inner bank.

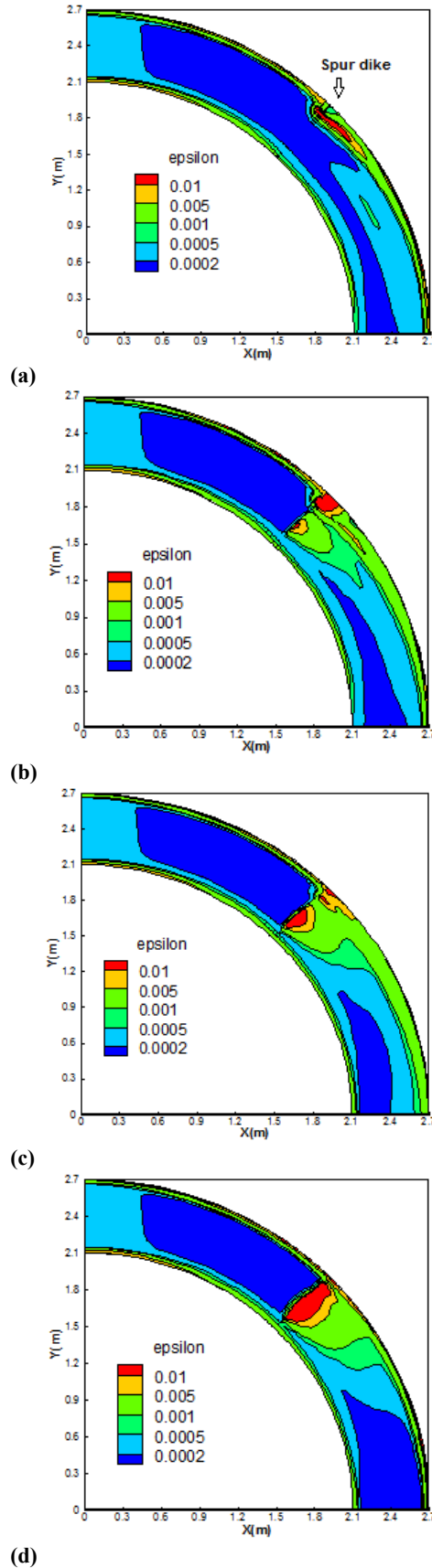


Fig. 7. Loss of kinetic energy on the water surface at submergence ratios of: (a) 0%, (b) 5%, (c) 25%, and (d) 50%.

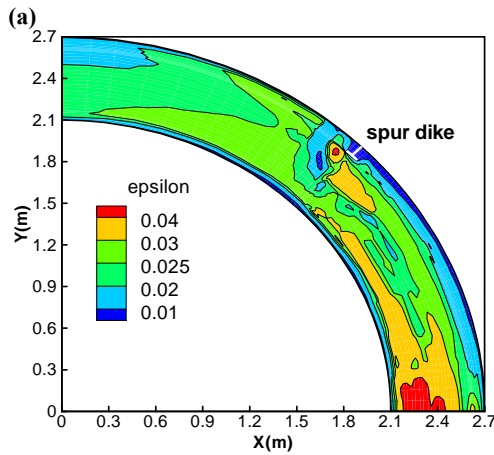
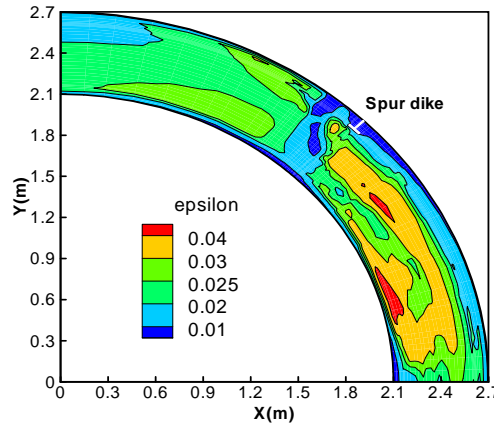


Fig. 8. Loss of kinetic energy near the bed at submergence ratios of: (a) 0%, and (b) 25%.

According to Table 1, by increasing the submergence ratio, the eddy viscosity reduced near the bed. Note that in the figures, the inner and outer walls of the channel are marked in red and the beginning and the end of the bend are marked in blue, and these lines should not be mistaken for the legend line. After increasing spur dike submergence, more flow passes over the spur dike crest level and the vortices formed due to spur dike resistance against the flow become weaker. Therefore, flow velocity near the bed is reduced, resulting in a decrease in eddy viscosity.

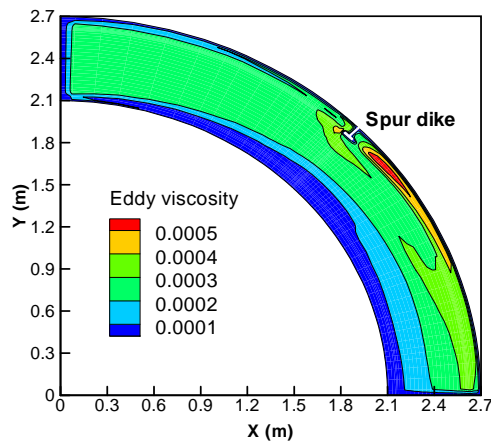


Fig. 9. Eddy viscosity on water surface with non-submerged spur dike.

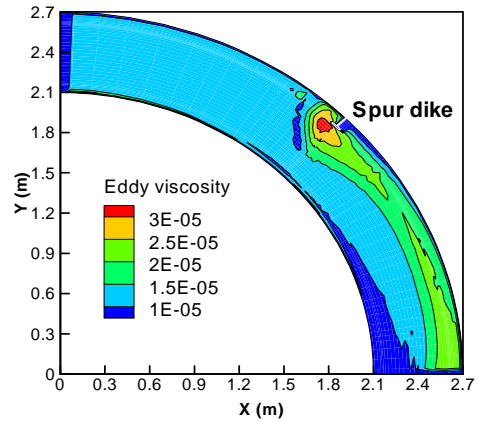


Fig. 10. Eddy viscosity near the bed with non-submerged spur dike.

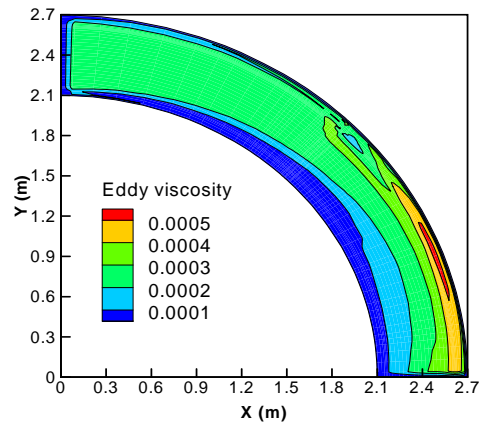


Fig. 11. Eddy viscosity on water surface at a 25% submergence ratio.

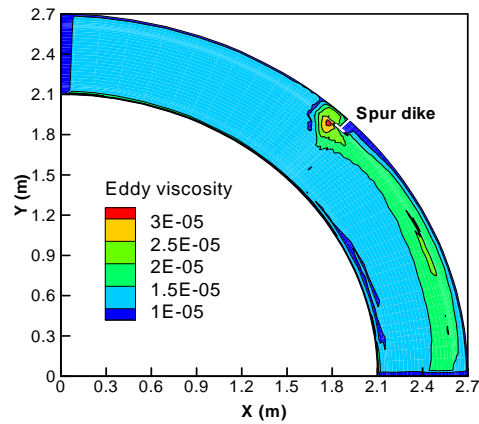


Fig. 12. Eddy viscosity near the bed at a 25% submergence ratio.

3.4 Pressure

As mentioned in Eq. (1), P is pressure. The SIMPLE method can be used for the equations of interlinked pressures. The main purpose of this method is to guess and select a value for the pressure, replace it in continuity equation and obtain the pressure correction factor. Then, the pressure correction factor is added to the initial pressure to satisfy the continuity equation. In this method, the pressure is not obtained directly, rather it is obtained through excessive accumulation of

pressure correction. Sometimes, this method will cause instability when calculating the pressure. The amount of the corrected pressure is multiplied in a smaller factor before adding to the pressure which is called the delay factor.

Table 1 Reduction in eddy viscosity at 1.25% distance of flow depth from the bed with increase in the submergence ratio

Change in submergence ratio (%)	Increase in eddy viscosity (%)	Change in submergence ratio (%)	Decrease in eddy viscosity (%)
From 0 to 5	3	From 5 to 25	9
From 0 to 15	8	From 5 to 50	40
From 0 to 25	11	From 15 to 25	3
From 0 to 50	42	From 15 to 50	36
From 5 to 15	6	From 25 to 50	34

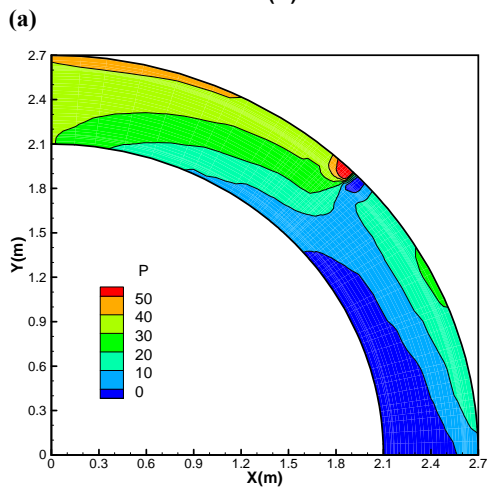
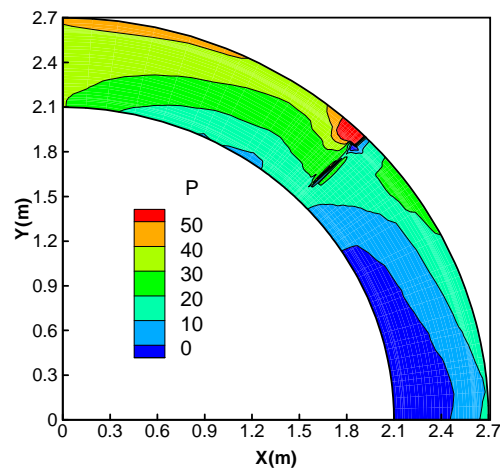


Fig. 13. Pressure distribution on water surface at submergence ratios of: (a) 5%, and (b) 25%.

As shown in Figs. 13 and 14, the changes of pressure are shown at different submergence ratios near the bed and water surface. During the collision of flow to the spur dike, the velocity head becomes equal to zero and is converted to pressure consequently. This will increase the pressure at the upstream end of the spur dike.

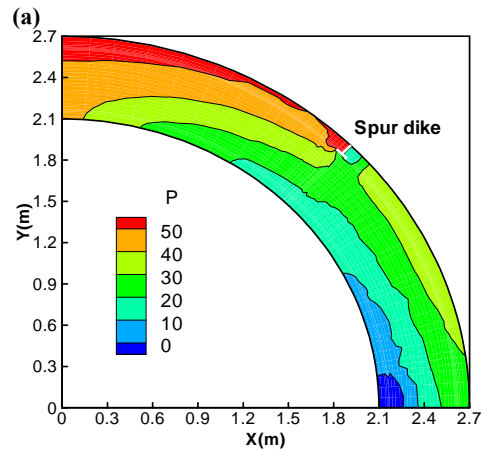
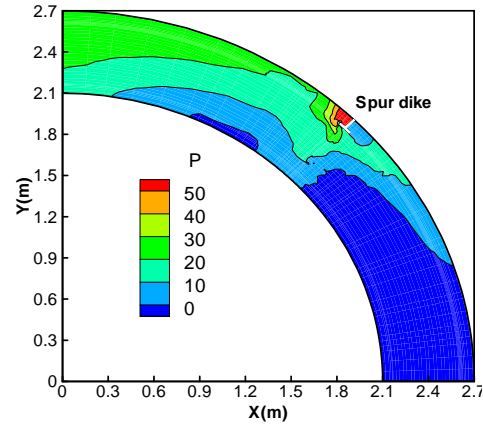


Fig. 14. Pressure distribution near the bed at submergence ratio of: (a) 0%, and (b) 50%.

Near the bed, at all submergence ratios, the maximum pressure occurs at the upstream end of the spur dike. Near the bed, and also at the water surface, by increasing the submergence ratio, the negative pressure range is reduced at the inner bank of the bend exit, but the changes in pressure at the bed and water surface are uptrend. In submergence mode, as the flow passes over the spur dike crest level and the velocity gradient changes, the pressure of water surface will change drastically from the outer wing of the spur dike toward the inner bank due to changes in water surface.

3.5 Froude Number

In a straight channel, when the flow has not yet entered the channel bend and not yet affected by back water phenomena, the height of water is assumed constant and the flow is steady. Therefore, the Froude number which is a function of flow depth can be considered constant upstream, but upon the arrival of the flow to channel bend,

Table 2 Changes in the minimum Froude number based on the changes in submergence ratio

Submergence ratio (%)	Increase in the minimum Froude number (%)	Submergence ratio (%)	Increase in the minimum Froude number (%)
From 0 to 5	194	From 5 to 25	197
From 0 to 15	319	From 5 to 50	332
From 0 to 25	380	From 15 to 25	120
From 0 to 50	640	From 15 to 50	200
From 5 to 15	165	From 25 to 50	169

Table 3 Changes in Froude number based on the spur dike submergence at the inner bank of the bend exit

Submergence ratio (%)	Increasing the maximum Froude Number	Submergence ratio (%)	Increasing the maximum Froude Number
From 0 to 5	7	From 5 to 25	84
From 0 to 15	19	From 5 to 50	97
From 0 to 25	96	From 15 to 25	65
From 0 to 50	110	From 15 to 50	77
From 5 to 15	11	From 25 to 50	7

affected by secondary flow and backwater phenomena, the flow depth has changed and will change the Froude number. As shown in Figs. 15 and 16, these changes are specified for different submergence ratios.

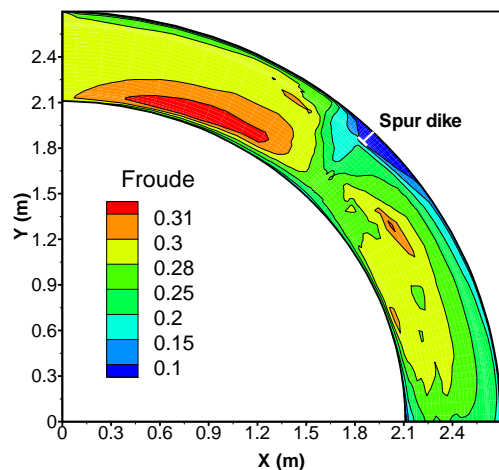


Fig. 15. Froude number at a 5% submergence ratio.

At all submergence ratios, the minimum Froude number is observed near the downstream and upstream ends of the spur dike, because the relationship between the flow depth with Froude number and flow velocity, leads to reduction in the Froude number. By changing the submergence ratio, the maximum Froude number does not change significantly, but the minimum Froude number increases by increasing the submergence ratio as in Table 2. This means that the minimum Froude number increases near the upstream and downstream ends of the spur dike, which is due to the high flow velocity and lower blockage of the flow in this region. As shown in Table 3, by increasing the submergence ratio, the Froude number increases near the inner bank at the bend exit. There is a low velocity at the upstream and downstream ends of the spur dike due to spur dike effect, and thus the Froude number which depends on flow velocity also decreases. Upon increasing spur dike submergence, more flow passes over the spur dike crest, thus increasing flow velocity and the Froude number; hence, the effect of spur dike on diverting the flow from the outer bank and preventing the outer bank erosion is evident.

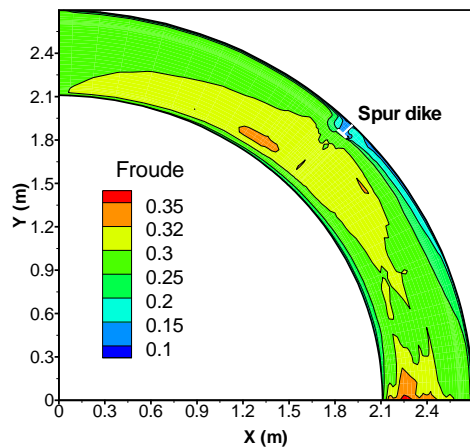


Fig. 16. Froude number at a 50% submergence ratio.

4. CONCLUSION

After examining the effective parameters of turbulent flow in a curved channel with moving bed, and by modeling a T-shaped spur dike at different submergence ratios at the middle of the outer bank, the results can be seen below:

- By increasing the submergence ratio near the bed, the amount and range of kinetic energy are reduced near the wing of the spur dike.
- Near the bed, for all submergence ratios, the maximum pressure occurs at the upstream end of the spur dike. Also, in this region, by increasing submergence ratio on water surface, the negative pressure range is reduced in the inner bank of bend exit.
- For all submergence ratios, the lowest Froude number is observed near the downstream and upstream ends of the spur dike. By increasing the submergence ratio from 0 to 50%, the Froude number increases 2.1 times at the inner bank of bend exit.
- By increasing the submergence ratio from 0% (non-submerged) to 50%, the value of eddy viscosity near the bed is reduced by 42%.

REFERENCES

- Abhari, M., M. Ghodsian, M. Vaghefi and N. Panahpur (2010). Experimental and numerical simulation of flow in a 90° bends. *Flow Measurement and Instrumentation* 21(3), 292-298.
- Basser, H., H. Karami, S. Shamshirband, S. Akib, M. Amirmojahedi, R. Ahmad, A. Jahangirzadeh and H. Javidnia (2015). Hybrid ANFIS-PSO approach for predicting optimum parameters of a protective spur dike. *Applied Soft Computing* 30, 642-649.
- Duan, J. G., L. He, Q. Wang and X. Fu (2011). Turbulent burst around experimental spur dike. *International Journal of Sediment Research* 26(4), 471-523.
- Elçi, S. and B. Ekmekçi (2016). Observational and numerical methods for quantifying and modeling of turbulence in a stratified reservoir. *Journal of Applied Fluid Mechanics* 9(4), 1603-1614.
- Falahatkar, S. and H. Ahmadikia (2014). Thermal analysis of superheater platen tubes in boilers. *Journal of Applied Fluid Mechanics* 7(2), 197-208.
- Fang, H., J. Bai, G. He and H. Zhao (2013). Calculations of non-submerged groin flow in a shallow open channel by Large-Eddy Simulation. *Journal of Engineering Mechanics* 140(5).
- Mayerle, R., F. M. Toro and S. S. Y. Wang (1995). Verification of a three-dimensional numerical model simulation of the flow in the vicinity of spur dikes. *Journal of Hydraulic Research* 33, (2), 243-256.
- McCoy, A. W. (2006). *Numerical investigations using LES: exploring flow physics and mass exchange processes near groynes*. Ph. D. thesis, The University of Iowa, Iowa, USA.
- Olsen, N. R. B. (1999). *Computational fluid dynamics in hydraulic and sedimentation engineering*. Class notes, 2nd. Revision, Norwegian University of Science and Technology, Norway.
- Olsen, N. R. B. (2000). *CFD algorithms for hydraulic engineering*. Norwegian University of Science and Technology, Norway.
- Olsen, N. R. B. (2001). *CFD modeling for hydraulic structures*. 1st edition, Norwegian University of Science and Technology, Norway.
- Olsen, N. R. B. (2009). *A three-dimensional numerical model for simulation of sediment movement in water intakes with multi block option*. Department of hydraulic and environmental engineering. User's manual, Norwegian University of Science and Technology, Norway.
- Rajaratnam, N. and B. A. Nwachukwu (1983). Flow near Groin-like Structures. *Journal of Hydraulic Engineering* 109(3), 463-480.
- Shukry, A. (1950). Flow around bends in an open flume. *Transactions of the American Society of Civil Engineers* 115(1), 751-779.
- Sukhodolov, A., C. Engelhardt, A. Krüger and H. Bungartz (2004). Case study: turbulent flow and sediment distributions in a groyne field. *Journal of Hydraulic Engineering* 130(1), 1-9.
- Vaghefi, M., M. Akbari, A. R. Fiouz (2016). An Experimental study of mean and turbulent flow in a 180 degree sharp open channel bend: secondary flow and bed shear stress. *KSCE Journal of Civil Engineering* 20(4), 1582-1593.

- Vaghefi, M., M. Ghodsian and S. A. A. Salehi Neyshabouri (2009). Experimental study on effect of T-shape spur dike length on scour in a 90° channel bend. *The Arabian Journal for Science and Engineering* 34(2), 337-345.
- Vaghefi, M., M. Ghodsian and S. A. A. Salehi Neyshabouri (2012). Experimental study on scour around a T-shaped spur dike in a channel bend. *Journal of Hydraulic Engineering* 138 (5), 471-474.
- Vaghefi, M., M. Shakerdargah and M. Akbari (2014). Numerical investigation of the effect of Froude number on flow pattern around a submerged T-shaped spur dike in a 90° bend. *Turkish Journal of Engineering and Environmental Sciences* 38(2), 266-277.
- Vaghefi, M., V. Mohseni Mehr and M. Akbari (2014). Numerical investigation of wing to web length ratios parameter of T-shaped spur dike in a 90° bend on scour pattern. *Journal of River Engineering* 2(3), 1-8.
- Vaghefi, M., Y. Safarpour and M. Akbari (2015). Numerical investigation of flow pattern and components of three-dimensional velocity around a submerged T-shaped spur dike in a 90 degree bend. *Journal of Central South University*, In Press.
- Vaghefi, M., Y. Safarpour and S. S. Hashemi (2015). Effects of relative curvature on the scour pattern in a 90° bend with a T-shaped spur dike using a numerical method. *International Journal of River Basin Management* 13(4), 501-514.
- Wildhagen, J. (2004). *Applied computational fluid dynamics with sediment transport in a sharply curved meandering channel*. Institute for Hydromechanics, University of Karlsruhe (TH), Germany.
- Yazdi, J., H. Sarkardeh and H. M. D. Azamathulla, (2010). 3D simulation of flow around a single spur dike with free-surface flow. *International Journal of River Basin Management* 8(1), 55-62.
- Zhang, H., H. Nakagawa, K. Kawaike and B. A. B. A. Yasuyuki (2009). Experiment and simulation of turbulent flow in local scour around a spur dyke. *International Journal of Sediment Research* 24(1), 33-45.